
Human-Object Interaction from Human-Level Instructions

Zhen Wu, Jiaman Li, C. Karen Liu
Stanford University

Abstract

Intelligent agents need to autonomously navigate and interact within contextual environments to perform a wide range of daily tasks based on human-level instructions. These agents require a foundational understanding of the world, incorporating common sense and knowledge, to interpret such instructions. Moreover, they must possess precise low-level skills for movement and interaction to execute the detailed task plans derived from these instructions. In this work, we address the task of synthesizing continuous human-object interactions for manipulating large objects within contextual environments, guided by human-level instructions. Our goal is to generate synchronized object motion, full-body human motion, and detailed finger motion, all essential for realistic interactions. Our framework consists of a large language model (LLM) planning module and a low-level motion generator. We use LLMs to deduce spatial object relationships and devise a method for accurately determining their positions and orientations in target scene layouts. Additionally, the LLM planner outlines a detailed task plan specifying a sequence of sub-tasks. This task plan, along with the target object poses, serves as input for our low-level motion generator, which seamlessly alternates between navigation and interaction modules. We present the first complete system that can synthesize object motion, full-body motion, and finger motion simultaneously from human-level instructions. Our experiments demonstrate the effectiveness of our high-level planner in generating plausible target layouts and our low-level motion generator in synthesizing realistic interactions for diverse objects. Please refer to our project page for more results: hoifhli.github.io.

1 Introduction

Synthesizing human-object interactions within contextual environments is pivotal across diverse fields such as computer graphics, embodied AI, and robotics. When tasked with human-level instructions, intelligent agents must first comprehend these high-level commands before they can carry out the necessary action sequences. For instance, if instructed to set up a workspace in a bedroom, an agent must understand the abstract concept of “workspace”, identify the available furniture/objects in the scene relevant to the concept, and translate the concept into a series of concrete actions, such as moving and orienting a desk, placing a chair nearby, and setting a monitor on the desk. In addition to understanding human-level instructions, the agent must emulate realistic human movements and interactions. This includes navigating through cluttered spaces, manipulating various objects, and appropriately releasing them after use. Moreover, accurately simulating detailed finger motions is essential for achieving truly lifelike manipulation behaviors.

Prior research has made significant strides in synthesizing long-horizon human-scene interactions using LLM planners [49]. However, most interactions have been limited to static objects without hand manipulation. Some work [23] demonstrated manipulation of dynamic objects, but the resulting interactions still lack realistic finger movements. Synthesizing full-body and finger movements together from human-level instructions while tackling both navigation and manipulation problems is

challenging for two primary reasons. First, human-level instructions typically provide only a broad outline of tasks, requiring common sense and world knowledge to transform these instructions into precise spatial object arrangements and detailed task plans. Second, existing datasets with paired full-body and finger motion data are limited to interactions with small objects and lack locomotion while manipulating objects [38, 9]. While a recent dataset [24] includes locomotion and manipulation for large objects, it does not contain detailed finger movements due to the difficulty of acquiring data for both modalities simultaneously.

To tackle the challenge of comprehending human-level instructions, we utilize the latest advancements in vision-language models (VLMs) and large language models (LLMs), which are highly effective in processing and interpreting both visual and textual information [31, 26]. However, LLMs are not well-suited for predicting precise scene layouts, such as the specific positions and orientations of objects. Instead of directly prompting LLMs to specify object placements, we utilize object spatial relationships as intermediate representations and ask LLMs to derive these relationships from the human-level instructions provided. From the intermediate representations, we could develop an algorithm to systematically convert the high-level plan to executable actions performed by the low-level motion generator.

To address the lack of large-scale object manipulation datasets with synchronized full-body and finger motions, one could use separate datasets to train a model for full-body motion manipulation without fingers and another model for finger-object manipulation. However, a causality dilemma emerges when putting the motions together from two models—should we first generate the full-body manipulation and then enforce the finger-object contacts to agree with the wrist poses determined by the full-body motion, or should we first generate the detailed finger motion with precise finger-object contacts and then generate the full-body motion consistent with the wrist poses from the finger motion? The former would result in glaring physical artifacts at finger-object contacts while the latter requires the object motion of full-body manipulation be known during finger motion generation. Our solution to break the dilemma is to employ *both* approaches in three steps. We first generate full-body and object motions without detailed fingers. The object motion and rough wrist poses provide guidance for generating contact-consistent finger motion in the second step. Finally, we generate full-body and object motions again conditioned on precise finger motions. Additionally, we train another model to generate smooth finger transition motions during the pre-contact and post-contact phases. Since contact satisfaction is not considered in these phases, we can use any hand-only manipulation dataset to train the model and attach the finger motion directly to full-body motion. Our framework successfully produces synchronized object motion, full-body motion, and finger motions, circumventing the need for a dataset with all data modalities.

To summarize, our work makes the following contributions. First, we develop a complete system capable of synthesizing continuous human-object interactions with intricate finger movements, driven by human-level instructions. Second, we leverage LLM and VLM for precise spatial task planning grounded by executable actions. Third, we propose an effective low-level motion generator that synthesizes contextual human motions with full-body navigation and manipulation, as well as detailed finger interaction with objects.

2 Related Work

Contextual Interaction Synthesis. Recent work on modeling human-object interactions can be divided into two paradigms: interactions with static objects and interactions with dynamic objects. Synthesizing human motions in static 3D scenes has been extensively studied, leveraging datasets with paired scene and human motion data [13, 46, 2, 20] and paired object and human motion data [12]. Prior research has explored regression models [43, 42, 12, 2, 30] and diffusion models [18, 20, 53, 45] to generate human motions interacting with 3D scenes, such as sitting on a chair or lying down on a sofa. Some studies have also explored reinforcement learning methods to generate physically plausible human motions [14, 56, 49]. These works focus on static objects, whereas our work focuses on dynamic interactions.

There has been increasing attention on synthesizing human-object interactions with dynamic objects. Prior work collected a large-scale motion capture dataset for dynamic human-object interactions and proposed a framework to synthesize human motions from object motions [24]. InterDiff [50] predicts future interaction motions based on past object and human motion. Several studies have employed

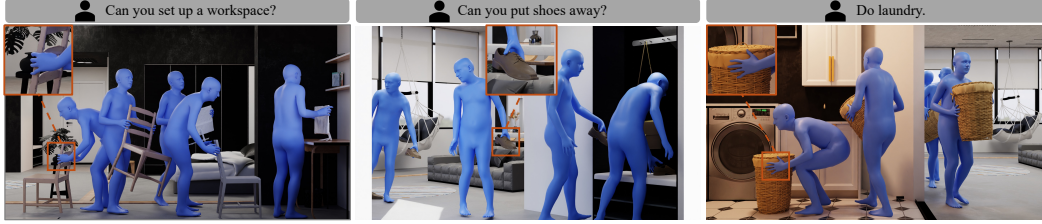


Figure 1: Given human-level instructions, we generate synchronized full-body human motion, finger motion, and object motion to accomplish the task.

conditional diffusion models to generate human-object interactions from language descriptions [7, 32, 47, 51], using paired text and interaction motion data from BEHAVE [3]. Another study, CHOIS [23], tackles the task of synthesizing human-object interactions from text within 3D scenes, using sparse waypoints to ground the interaction synthesis in the environment. Despite these advancements, all of these works focus on full-body human motion generation without detailed hand motions. In this work, we aim to generate synchronized object motions, human motions, and finger motions.

Hand-Object Interaction Synthesis. Hand-object interaction synthesis has been extensively explored in computer graphics, computer vision, and robotics. In the realm of static pose generation, traditional methods often rely on physics-based control or optimization techniques to generate grasp candidates [25, 33, 36]. Some recent work utilize differentiable force closure estimators to generate high-quality grasp pose [44, 27]. Moreover, recent advancements have pivoted towards data-driven approaches, leveraging deep learning to directly estimate hand grasps from extensive interaction datasets [19, 4, 22, 38, 6]. Going beyond static grasp generation, another line of work also explores dynamic object manipulation [55, 52, 28]. ManipNet [55] introduces a spatial representation based on the hand-object distance, then trains an auto-regressive model to generate finger movement.

Recent works further explore integrating whole-body motion and hand motion [39, 40, 48, 37]. IMoS [10] generates hand-object interaction using the GRAB dataset [38] with paired human motion and hand motion. [5] leverage reinforcement learning to achieve physically plausible motion. However, these methods are constrained to manipulate small-sized objects in GRAB [38], unable to generate both full-body human motions and finger motions for large-sized objects. In this work, we aim to generate realistic full-body human motion and finger motions for manipulating large-sized objects. As there is no large-scale dataset with both full-body human motion and finger motion, we leverage DexGraspNet [44] to generate a realistic grasp pose for the contact phase, train a conditional diffusion model on GRAB [38] to generate approaching and releasing finger motions, and then integrate our full-body motion generation with the generated finger motions.

LLM-based Planning. LLMs have been extensively used to address various reasoning and planning tasks [16, 17, 41, 54, 8]. Previous work has leveraged LLMs to generate detailed task plans for robots [17, 41] and to tackle object arrangement tasks where target object positions need to be specified [54, 8]. Recent work in indoor scene layout generation [1] uses LLMs to create room layouts where object positions and orientations are precisely determined.

In addition, LLMs have been adopted in motion synthesis tasks for their high-level planning capabilities. UniHSI [49] uses LLMs to extract action plans in a chain-of-contact format, guiding a low-level controller to synthesize corresponding motions. InterDreamer [51] employs LLMs to identify object parts that humans interact with and uses this information to retrieve initial human poses. CHOIS [23] uses LLMs to extract key information to determine target object position, deriving sparse waypoints as input for a conditional diffusion model to generate interactions grounded in scenes. However, CHOIS requires explicit language descriptions (e.g., "Lift the monitor, move, and put it on the desk.") as input, which cannot support interaction synthesis from more abstract human-level instructions (e.g., "Set up a workspace"). In this work, we utilize LLMs to process human-level instructions, providing detailed task plans and target scene layouts. This information will guide our low-level interaction synthesis.

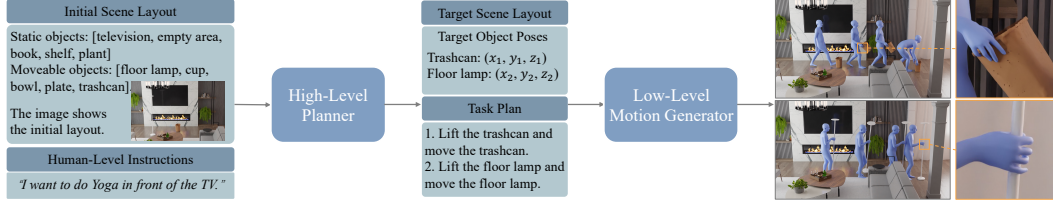


Figure 2: Our system takes the initial scene layout and human-level instruction as input, and uses a high-level planner to obtain the target scene layout and a detailed task plan. The low-level motion generator then generates synchronized object motion, full-body human motion and finger motion.

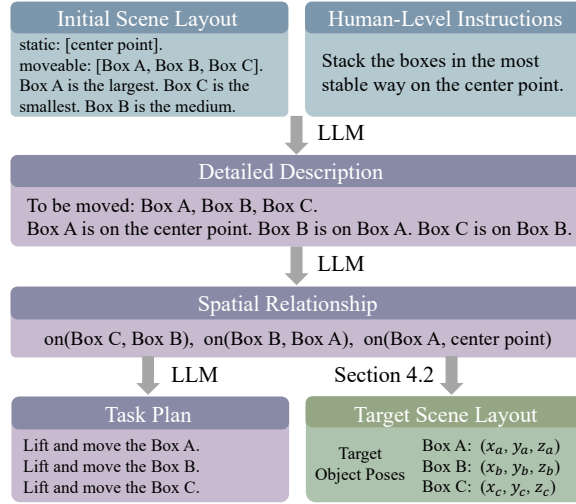


Figure 3: The high-level planner utilizes LLMs to reason about the human-level instructions and generates a target scene layout and a task plan executable by the low-level motion generator.

3 System Overview

Given a human-level instruction and an initial scene layout description, we develop a system that generates synchronized human motion and object motion to accomplish the task in the scene through navigation and manipulation. The initial layout describes a list of objects in a 3D scene and their spatial relationships, while the human-level instruction is provided as an abstract description of a task that requires grounded reasoning based on world knowledge and common sense.

An overview of our system is depicted in Figure 2. The system comprises two main components: a high-level planner and a low-level motion generator. The high-level planner leverages a large language model (LLM) to interpret the instructions and generate both target scene layouts and detailed task plans, as discussed in Section 4. These layouts specify the desired positions and orientations of the objects, while the task plans outline the steps for interacting with these objects. The low-level motion generator creates the actual motion sequences that include both object and human movements, emphasizing realistic human-object interactions and navigation within the scene. The motion generator consists of an interaction module and a navigation module. The interaction module, introduced in Section 5.1, employs an effective multi-stage framework to produce lifelike interaction motions. The navigation module, described in Section 5.2, uses a conditional diffusion model to generate walking motions guided by the positions and orientations of the waypoints. The interaction module and the navigation module operate sequentially, incorporating a strategy designed to ensure natural transitions between the two.

4 High-Level LLM Planner

Given a human-level instruction, the planner has two primary objectives: to compute the specific target layout based on the instruction and to generate a detailed task plan outlining how and in what order each object should be moved. Inputs to the high-level planner consist of an initial scene layout

\mathcal{S} and human-level instructions \mathcal{I} , both of which can be images, texts, or a combination of both. We also specify which objects are movable in \mathcal{S} . Outputs to the high-level planner comprise the target layout and the task plan. The target layout specifies the target position p and orientation q for each object o that requires movement, represented as $\{\{o_1, p_1, q_1\}, \dots, \{o_n, p_n, q_n\}\}$. The task plan is a sequence of text actions, denoted as $\{l_1, l_2, \dots, l_T\}$, where each text action l_t is a short-horizon language instruction (e.g., “move the monitor”) specifying a sub-task.

While the most straightforward method to generate the target layout is to directly ask LLMs to explicitly specify all object positions and orientations, recent research suggests that LLM’s 3D reasoning abilities are not yet reliable [1, 16], even with the state-of-the-art LLMs like OpenAI’s GPT-4. To increase LLM’s reliability in spatial reasoning for our tasks, we use a similar in-context learning strategy inspired by previous work [1], and propose a method to ensure LLM’s answers are actionable by the low-level motion generator. Specifically, we first prompt the LLM to give a detailed description of the scene in natural language. Subsequently, we ask the LLM to identify a set of relevant objects and describe their spatial relationships using a predefined set of spatial predicates. From there, a simple method is proposed to automatically compute the specific object positions and orientations. We also implement a process as a guardrail against the event when the LLM’s answers lead to collisions in the scene or lack sufficient information to determine the precise position and orientation of the object.

Overall, our planner consists of three stages:

1. Generate spatial relationships between objects (Section 4.1).
2. Calculate target layouts (Section 4.2).
3. Generate detailed task plans (Section 4.3).

Figure 3 shows a schematic of this pipeline. The remainder of this section describes each stage in more detail.

4.1 Spatial Relationship Generation

Given a human-level instruction, the first stage of the high-level planner utilizes LLMs to obtain target spatial relationships between objects. Following [1], we define the following relation functions to describe the spatial relationships. We found that these three relationships are sufficient to address most rearrangement tasks in a typical home environment, although our framework remains flexible to include additional relationships if necessary.

1. `on(object1, object2)` indicates that `object1` is positioned on top of `object2`.
2. `adjacent(object1, object2, direction, distance)` determines the adjacency between `object1` and `object2`, with optional parameters, `direction` and `distance`, to specify the relative orientation and separation.
3. `facing(object1, object2)` denotes that `object1` is oriented towards `object2`.

For example, if a monitor needs to be put on the table facing the chair, we can use `on(monitor, table)` and `facing(monitor, chair)` to describe its pose. If a table is positioned 1 meter to the north of the door, we can use `adjacent(table, door, north, 1)` to describe the relationship. The "on" and "adjacent" functions can later be translated to 3D coordinate offsets to calculate object positions from known object positions. Specifically, if object o_1 is "on" object o_2 , whose position is known, then o_1 ’s height is set to match the top surface of o_2 , while the x - y coordinates are sampled within the x - y range of o_2 without overlapping with other objects. If o_1 is "adjacent" to o_2 , and the direction and distance are given by LLMs, we directly use those values as the offset. Otherwise, we sample a random position around o_2 . A post-process is applied to ensure no overlap between objects.

We prompt LLMs to generate the objects that need to be moved and their spatial relationships. Following [1], we first let LLMs generate a detailed natural language description of the spatial relationships, then translate it into specific relation functions. In-context learning is employed during the process to assist LLMs to better understand the requirements. We provide complete prompts for the LLM planner in the supplementary materials.

4.2 Target Layout Calculation

The target layout can then be calculated given the spatial relationships. We propose an algorithm that we find highly effective in handling typical indoor room scenes.

Firstly, we compute positions by constructing a scene graph [21] using the given relationships. In this graph, each node represents an object, and each edge represents the relationships. The edges are directional, pointing from `object2` to `object1`, and primarily consider 'on' and 'adjacent' relationships. The orientation relation, enforced by 'facing', will be addressed in the subsequent step. Nodes are categorized as M nodes (to be moved) or S nodes (static) based on whether they need to be moved in the task plan provided by LLMs in the previous step. The algorithm employs a method similar to topological sorting. We start by marking all S nodes as P (processed). Assuming no cycles are present in the graph, we first process the M nodes that have only incoming edges from P nodes. The position of each M node is determined by adding a predefined offset to the known position of the connected P node, based on the type of spatial relationship (see 4.1). For M nodes connected to multiple P nodes, the average of positions computed from the P nodes is used. Once calculated, the position of the M node is determined and marked as P . This process is repeated until all nodes are processed. This method effectively handles the majority of cases encountered. For cases with cycles in the graph, we identify the M node with the most relationships with known-position nodes in the cycle, remove its incoming edges from unprocessed nodes, and transform the graph into a cycle-free structure.

Next, we compute orientations. For an object o , we pre-calculate its facing direction d . Then, based on the `facing(o, t)` relationship, the facing direction \hat{d} is determined as the direction from object o to object t . Thus, the object's orientation is defined by $R(\hat{d})R(d)^{-1}$.

4.3 Task Plan Generation

The final stage of the planner receives all previous outputs and generates the detailed task plan using LLMs. The task plan consists of a sequence of textual actions, denoted as $\{l_1, l_2, \dots, l_T\}$, where each textual action l_t specifies a sub-task involving interaction with an object. The LLMs are prompted to describe each interaction task and determine the order of the interactions, which is crucial for achieving natural interaction motion. For example, if a vase is on a table, we need to first move the vase before moving the table. The LLMs are asked to generate the most natural order of actions to ensure seamless and realistic task execution, and to explain their reasoning.

To enable the human to execute the task plan, i.e., to move next to the object and relocate it to the target position, we use an A* planner to automatically generate collision-free paths in the scene. The path is represented as a series of waypoints, which will later serve as inputs for the low-level motion generator.

5 Low-Level Motion Generator

Given the target scene layouts and task plans generated by the high-level planner, our low-level motion generator executes the interaction module and navigation module sequentially to generate continuous navigation motions and human-object interactions.

5.1 Interaction Module

We introduce a multi-stage interaction module that synthesizes full-body and finger movements, synchronized with the object motion (Figure 4). The first stage generates initial human and object motions without detailed finger motion using the pre-trained CHOIS model [23], referred to as CoarseNet. Observing that the wrist usually maintains a consistent relative pose with respect to the object when they are in contact, we propose to use a state-of-the-art grasp pose generation method [44] to obtain an optimized grasp pose. However, the optimized grasp pose cannot be directly integrated back into the human motion generated by CoarseNet because the wrist positions from the first stage are likely to be different from those optimized in the second stage. To address the wrist misalignment issue, we introduce RefineNet, which takes the optimized wrist poses as an input condition and generates object and human motions that seamlessly align with them.

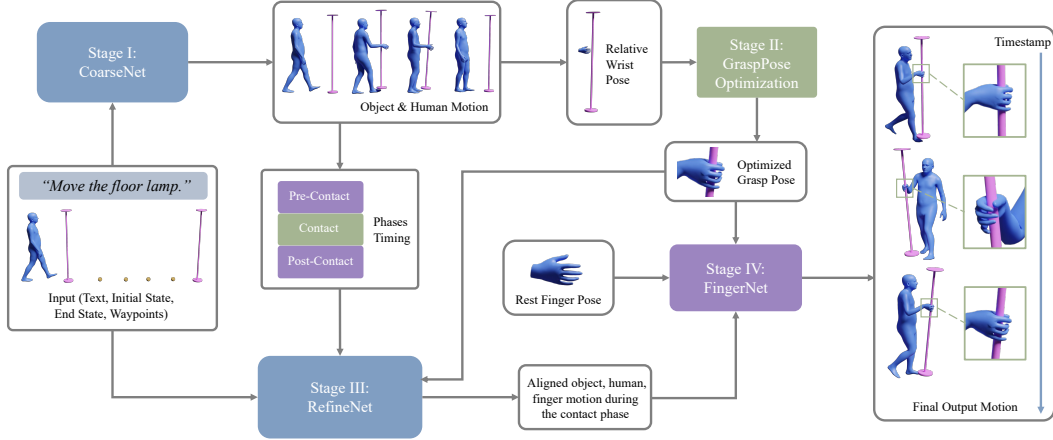


Figure 4: The interaction module consists of four stages. Starting from text, initial state, end state, and waypoints, CoarseNet generates the initial object and human motion. The relative wrist pose in the contact phase is used for an optimization to generate a valid grasp pose. Then RefineNet predicts object and human motion with more conditions to obtain refined motion that aligns with the relative wrist constraint. Finally, FingerNet completes finger motions.

From the first three stages, we obtain well-aligned motion when the object is in contact with the hands. However, we still need to synthesize detailed finger motions before the contact is established or after the contact is terminated. The last stage introduces a finger motion diffusion model, referred to as FingerNet, ensuring smooth finger motions for approaching and releasing the object, finalizing the interaction sequence.

5.1.1 CoarseNet

We utilize the pre-trained CHOIS model to generate synchronized object and human motions based on the initial state, end object state, sparse waypoints, object geometry, and text.

Motion Representation We denote human motion as $\mathbf{H} \in \mathbb{R}^{T \times D}$, where T represents the sequence length and D represents the dimension of the human pose. Each \mathbf{H}_t includes global joint positions and 6D continuous rotations [57], excluding finger joints. Object motion $\mathbf{O} \in \mathbb{R}^{T \times 12}$ includes the object’s global position and relative rotation matrix with respect to the input object geometry. The model also predicts contact labels $\mathbf{L} \in \mathbb{R}^2$ for both hands, which are used for test-time guidance.

Object Geometry Representation. Object geometry $\mathbf{G} \in \mathbb{R}^{1024 \times 3}$ is represented using the Basis Point Set (BPS) [34] method. This method involves sampling 1024 basis points from the volume of a ball with a 1-meter radius centered on the object. Directional vectors are then calculated from each basis point to the nearest point on the object, forming a compact BPS representation.

Input Condition Representation. The model uses a masked motion data representation $\mathbf{S} \in \mathbb{R}^{T \times (D+12)}$ to encode the initial states, end object state, and sparse waypoints. The initial state includes the human pose and object pose in the first frame, while the sparse waypoints provide a series of 2D object positions every 30 frames. Any remaining spaces in \mathbf{S} are padded with zeros. The masked motion data \mathbf{S} , the BPS representation \mathbf{G} , and text embeddings extracted by a pretrained CLIP model [35] together form the condition \mathbf{c} for the conditional diffusion model.

Conditional Diffusion Model. Training a diffusion model involves learning to reverse a forward diffusion process. Starting from clean data \mathbf{x}_0 , where $\mathbf{x}_0 = \{\mathbf{H}, \mathbf{O}, \mathbf{L}\}$, noise is progressively introduced until, after N steps, the data becomes approximately $\mathbf{x}_N \sim \mathcal{N}(0, \mathbf{I})$. The denoising network is trained to reverse this process so that sampling a noise \mathbf{x}_N and applying N denoising steps yields the clean data representation $\hat{\mathbf{x}}_0$. Each denoising step is defined as

$$p_\theta(\mathbf{x}_{n-1} | \mathbf{x}_n, \mathbf{c}) := \mathcal{N}(\mathbf{x}_{n-1}; \boldsymbol{\mu}_\theta(\mathbf{x}_n, n, \mathbf{c}), \sigma_n^2 \mathbf{I}), \quad (1)$$

where p_θ represents a neural network, $\boldsymbol{\mu}_\theta(\mathbf{x}_n, n, \mathbf{c})$ represents the learned mean, σ_n^2 denotes a fixed variance. The training loss is a reconstruction loss, $\|\hat{\mathbf{x}}_\theta(\mathbf{x}_n, n, \mathbf{c}) - \mathbf{x}_0\|_1$.

The conditional diffusion model uses input conditions c to generate object motion O , human motion H , and hand contact L . To ensure realistic hand-object contact and reduce artifacts, CHOIS employs test-time guidance [15] to minimize wrist-object distance in the contact phase, feet-floor distance, and penalize object-floor penetration. For more details, please refer to [23].

5.1.2 Grasp Pose Generation

The output of CoarseNet provides coordinated full-body and object motion, but the hands maintain a rest pose throughout the motion, resulting in visually and physically implausible hand-object contacts. We address this issue in the second stage by applying a state-of-the-art grasp pose generation method [44] to obtain a detailed grasp pose with accurate finger-object contact.

Based on the object’s velocity in the first stage, we segment the generated interaction sequence into pre-contact, contact, and post-contact phases, where the object velocities in the pre-contact and post-contact phases are approximately zero. We also use the average relative wrist pose computed from Stage 1 to generate a plausible grasp pose as an initial guess to be optimized. Starting with an object mesh and the initial hand pose $g = (T, R, \theta)$, where $T \in \mathbb{R}^3$ and $R \in SO(3)$ represent the wrist position and rotation in the object’s frame, and $\theta \in \mathbb{R}^{45}$ represents the finger configuration, we formulate an optimization to compute a hand pose that minimize a differentiable force closure energy term and a regularization term (details in [44]). For motions involving both hands, such as carrying a box, we omit the force closure term because the grasp stability does not rely solely on the fingers of one hand. The optimized grasp pose is denoted by $\hat{g} = (\hat{T}, \hat{R}, \hat{\theta})$. The optimized wrist pose $\hat{w} = (\hat{T}, \hat{R})$ is subsequently used as the input condition for the third stage.

5.1.3 RefineNet

Given the optimized wrist pose \hat{w} from the second stage and the contact phase information, along with all the input conditions of CoarseNet, RefineNet generates human and object motions that align with the \hat{w} . This ensures that the generated full-body human motion seamlessly integrates with the grasp pose \hat{w} from the second stage.

Specifically, we encode the wrist pose and contact phase information by modifying the input masked data conditions (introduced in Section 5.1). We expand the data dimension to include an additional term representing the relative wrist pose. For the frames in the contact phase, the optimized wrist pose $\hat{w} \in \mathbb{R}^{T \times 18}$ includes the relative position and 6D orientation of both wrists. For the frames in the pre-contact and post-contact phases, we pad this term with zeros.

Additionally, we utilize RefineNet to further improve the object’s motion from Stage 1. Based on the fact that a stably placed object should be static when it is not in contact with the hand, during the pre-contact and post-contact phases, we modify the masked motion data representation S by replacing the object pose with the corresponding static pose and apply a post-processing step to further enforce this constraint (see more implementation details in the supplemental materials).

5.1.4 FingerNet

In this stage, we generate finger motions for the pre-contact and post-contact phases to form a complete interaction sequence. Given the start and end finger poses, along with the wrist trajectory in between, we employ a conditional diffusion model to predict the finger motions denoted as $F \in \mathbb{R}^{T \times D'}$, representing local joint 6D rotations [57].

Hand-Object Spatial Representation Similar to prior work [55, 39], we adopt a sensor representation to encode the spatial relationships between the hand and object. Specifically, we sample 100 vertices uniformly from the hand mesh on the palm side and compute their closest distance to the object surface. We denote this representation as $P \in \mathbb{R}^{T \times 100}$. The finger pose is assigned to the mean pose when calculating P .

Input Condition Representation We use a masked motion data representation $S \in \mathbb{R}^{T \times D'}$ to encode the start and end finger pose. Any remaining space in S is padded with zeros. The masked motion S and the sensor P then form the condition c for the model.

Finger Diffusion Model The FingerNet employs the same model architecture as CoarseNet, but is specifically tailored to process only the right hand. To generate finger motions for the left hand, we apply a mirroring strategy similar to [55]. Specifically, we first mirror the left hand and the corresponding object mesh to simulate a right-hand scenario. We then process this mirrored data to generate the finger motions. Finally, we mirror the resulting motions back to their original orientation to obtain the finger movements of the left hand.

5.2 Navigation Module

To generate long sequences of interaction with multiple objects, where humans move freely within a scene, we develop a navigation module for generating human locomotion based on waypoints.

This module, using a conditional diffusion model, predicts human motion ($\mathbf{H} \in \mathbb{R}^{T \times D}$) and feet-ground contact labels ($\mathbf{L}_f \in \mathbb{R}^{T \times 2}$). It conditions on the initial human pose, sparse waypoints, and textual inputs, integrating both the position and orientation (expressed as a normalized direction vector) of the waypoints to ensure consistent facing directions. Smooth transitions between the interaction and navigation modules are achieved by using the final pose of one module as the starting pose for the next.

6 Results

The qualitative results are best evaluated in the supplementary video. Here, we provide detailed information on additional experiments that assess the high-level planner and multi-stage interaction module.

6.1 Dataset and Evaluation Metrics

FullBodyManipulation The FullBodyManipulation dataset [24] contains 10 hours of object and human motion involving 15 objects. Both our RefineNet and the pretrained CoarseNet are trained on this dataset.

HumanML3D The HumanML3D dataset [11] includes 28 hours of diverse human motions accompanied by language descriptions. The human motion data are mostly derived from the large-scale motion capture dataset AMASS [29]. We train the navigation module on this dataset.

GRAB The GRAB dataset [38] contains full-body and finger motion data for 10 subjects interacting with 51 everyday objects, mostly small items. We train FingerNet using this dataset.

Evaluation Metrics We assess the condition matching accuracy and physical plausibility, using metrics from [23]:

- **Waypoints Matching Metric:** This metric calculates the Euclidean distance between predicted trajectories and input waypoints, including start (T_s) and end (T_e) object position errors, and waypoint errors (T_{xy}), all in centimeters (cm).
- **Interaction Quality Metric:** This evaluates interaction quality by measuring the contact proportion (C_p), which is the ratio of frames showing hand-object contact to total frames when the object is in motion. It also includes a penetration score (P_{hand}), which calculates the average depth at which the hand mesh penetrates the object mesh, in centimeters (cm).

6.2 Evaluation of High-Level Planner

Baselines We compare our target layout generation method to a baseline that employs LLMs to directly predict the object positions and orientations. Further details on the prompts are provided in the supplementary material.

Implementation Details We use OpenAI’s GPT-4V [31] for evaluating 15 tasks with human-level instructions. Both our method and the baseline are informed by detailed object information, including the center of mass and bounding box dimensions.



Figure 5: Comparisons of the target layout generation methods.

Results. We evaluate the baseline and our approach on 15 tasks and show a qualitative comparison example in Figure 5. The task involves setting up a workspace. The baseline method was unable to correctly position the monitor on the table; it also inaccurately determined the monitor’s facing direction. Detailed information on each task is provided in the supplementary material.

6.3 Evaluation of the Interaction Module

Baselines. We evaluate our multi-stage interaction module, which includes CoarseNet, RefineNet, and FingerNet, by comparing the closest previous work, CHOIS [23]. Since the CoarseNet alone is identical to CHOIS, we create the following three-way comparison: CoarseNet alone (CNet), CoarseNet combined with RefineNet but no FingerNet (C+RNet), and our method (C+R+FNet).

Results on the FullBodyManipulation dataset. We show a comparison in Table 1. Our multi-stage model generates realistic finger movements, ensuring more accurate contact and less penetration. The post-processing step in RefineNet further aligns the start and end states of the objects accurately.

To assess the models’ capability to generate long sequences, we test on randomly generated trajectories that support actions such as moving straight, turning, and executing U-turns, each approximately 10 meters long. The results are shown in Table 2, with qualitative comparisons provided in Figure 6.

Table 1: Quantitative Evaluation on FullBodyManipulation.

	$T_s \downarrow$	$T_e \downarrow$	$T_{xy} \downarrow$	$P_c \uparrow$	$P_{\text{hand}} \downarrow$
CNet	1.71	6.31	2.87	0.61	0.59
C+RNet	1.21	5.98	2.85	0.68	0.40
C+R+FNet (ours)	0.00	0.00	2.01	1.00	0.29

Table 2: Quantitative Evaluation on Long Trajectories.

	$T_s \downarrow$	$T_e \downarrow$	$T_{xy} \downarrow$	$P_c \uparrow$	$P_{\text{hand}} \downarrow$
CNet	4.38	5.37	3.14	0.59	0.31
C+RNet	3.48	5.22	4.36	0.64	0.27
C+R+FNet (ours)	0.00	0.00	2.43	1.00	0.20

7 Conclusion

To summarize, we have presented a complete system that synthesizes synchronized object motion, full-body human motion, and finger motion in contextual environments, driven by human-level instructions. Our framework consists of a high-level LLM planner and a low-level motion generator. The high-level LLM planner generates a target scene layout and a detailed task plan given an initial scene layout and high-level instructions. We have developed an effective multi-stage interaction module and navigation module to generate long-term human-object interactions with intricate finger movements, guided by the output from the planner.

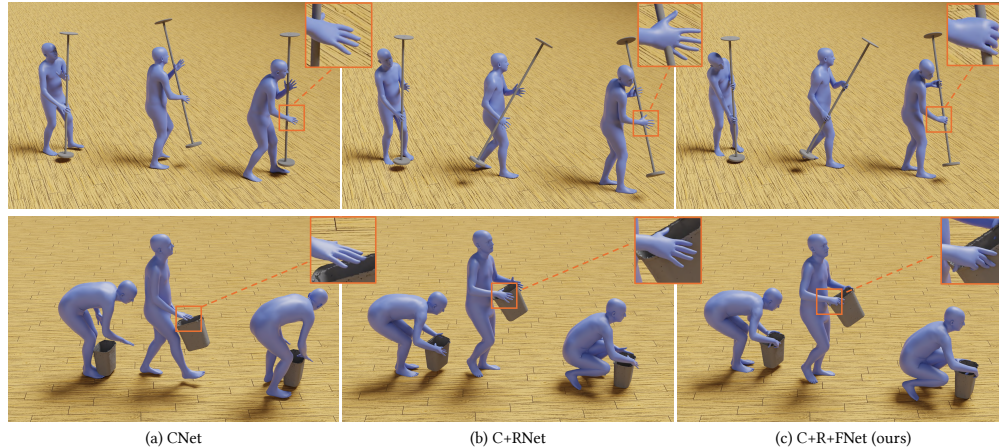


Figure 6: Qualitative comparisons of results for long trajectories.

References

- [1] R. Aguina-Kang, M. Gumin, D. H. Han, S. Morris, S. J. Yoo, A. Ganeshan, R. K. Jones, Q. A. Wei, K. Fu, and D. Ritchie. Open-universe indoor scene generation using llm program synthesis and uncurated object databases. *arXiv preprint arXiv:2403.09675*, 2024.
- [2] J. P. Araujo, J. Li, K. Vetrivel, R. Agarwal, D. Gopinath, J. Wu, A. Clegg, and C. K. Liu. Circle: Capture in rich contextual environments. In *Conference on Computer Vision and Pattern Recognition (CVPR)*, 2023.
- [3] B. L. Bhatnagar, X. Xie, I. A. Petrov, C. Sminchisescu, C. Theobalt, and G. Pons-Moll. Behave: Dataset and method for tracking human object interactions. In *Conference on Computer Vision and Pattern Recognition (CVPR)*, pages 15935–15946, 2022.
- [4] S. Brahmbhatt, A. Handa, J. Hays, and D. Fox. Contactgrasp: Functional multi-finger grasp synthesis from contact. In *2019 IEEE/RSJ International Conference on Intelligent Robots and Systems (IROS)*, pages 2386–2393. IEEE, 2019.
- [5] J. Braun, S. Christen, M. Kocabas, E. Aksan, and O. Hilliges. Physically plausible full-body hand-object interaction synthesis. *arXiv preprint arXiv:2309.07907*, 2023.
- [6] S. Christen, S. Hampali, F. Sener, E. Remelli, T. Hodan, E. Sauser, S. Ma, and B. Tekin. Diffh2o: Diffusion-based synthesis of hand-object interactions from textual descriptions. *arXiv preprint arXiv:2403.17827*, 2024.
- [7] C. Diller and A. Dai. Cg-hoi: Contact-guided 3d human-object interaction generation. *arXiv preprint arXiv:2311.16097*, 2023.
- [8] Y. Ding, X. Zhang, C. Paxton, and S. Zhang. Task and motion planning with large language models for object rearrangement. In *2023 IEEE/RSJ International Conference on Intelligent Robots and Systems (IROS)*, pages 2086–2092. IEEE, 2023.
- [9] Z. Fan, O. Taheri, D. Tzionas, M. Kocabas, M. Kaufmann, M. J. Black, and O. Hilliges. ARCTIC: A dataset for dexterous bimanual hand-object manipulation. In *Conference on Computer Vision and Pattern Recognition (CVPR)*, 2023.
- [10] A. Ghosh, R. Dabral, V. Golyanik, C. Theobalt, and P. Slusallek. Imos: Intent-driven full-body motion synthesis for human-object interactions. In *Computer Graphics Forum*, volume 42, pages 1–12. Wiley Online Library, 2023.
- [11] C. Guo, S. Zou, X. Zuo, S. Wang, W. Ji, X. Li, and L. Cheng. Generating diverse and natural 3d human motions from text. In *Proceedings of the IEEE/CVF Conference on Computer Vision and Pattern Recognition*, pages 5152–5161, 2022.
- [12] M. Hassan, D. Ceylan, R. Villegas, J. Saito, J. Yang, Y. Zhou, and M. Black. Stochastic scene-aware motion prediction. In *International Conference on Computer Vision (ICCV)*, pages 11354–11364, 2021.
- [13] M. Hassan, V. Choutas, D. Tzionas, and M. J. Black. Resolving 3d human pose ambiguities with 3d scene constraints. In *International Conference on Computer Vision (ICCV)*, pages 2282–2292, 2019.

- [14] M. Hassan, Y. Guo, T. Wang, M. Black, S. Fidler, and X. B. Peng. Synthesizing physical character-scene interactions. In *SIGGRAPH 2023 Conference Papers*, 2023.
- [15] J. Ho, T. Salimans, A. Gritsenko, W. Chan, M. Norouzi, and D. J. Fleet. Video diffusion models. *arXiv:2204.03458*, 2022.
- [16] Y. Hong, H. Zhen, P. Chen, S. Zheng, Y. Du, Z. Chen, and C. Gan. 3d-llm: Injecting the 3d world into large language models. *Advances in Neural Information Processing Systems*, 36:20482–20494, 2023.
- [17] Y. Hu, F. Lin, T. Zhang, L. Yi, and Y. Gao. Look before you leap: Unveiling the power of gpt-4v in robotic vision-language planning. *arXiv preprint arXiv:2311.17842*, 2023.
- [18] S. Huang, Z. Wang, P. Li, B. Jia, T. Liu, Y. Zhu, W. Liang, and S.-C. Zhu. Diffusion-based generation, optimization, and planning in 3d scenes. In *Conference on Computer Vision and Pattern Recognition (CVPR)*, 2023.
- [19] H. Jiang, S. Liu, J. Wang, and X. Wang. Hand-object contact consistency reasoning for human grasps generation. In *Proceedings of the IEEE/CVF international conference on computer vision*, pages 11107–11116, 2021.
- [20] N. Jiang, Z. Zhang, H. Li, X. Ma, Z. Wang, Y. Chen, T. Liu, Y. Zhu, and S. Huang. Scaling up dynamic human-scene interaction modeling. *arXiv preprint arXiv:2403.08629*, 2024.
- [21] J. Johnson, R. Krishna, M. Stark, L.-J. Li, D. Shamma, M. Bernstein, and L. Fei-Fei. Image retrieval using scene graphs. In *Proceedings of the IEEE conference on computer vision and pattern recognition*, pages 3668–3678, 2015.
- [22] K. Karunratanakul, J. Yang, Y. Zhang, M. J. Black, K. Muandet, and S. Tang. Grasping field: Learning implicit representations for human grasps. In *2020 International Conference on 3D Vision (3DV)*, pages 333–344. IEEE, 2020.
- [23] J. Li, A. Clegg, R. Mottaghi, J. Wu, X. Puig, and C. K. Liu. Controllable human-object interaction synthesis. *arXiv preprint arXiv:2312.03913*, 2023.
- [24] J. Li, J. Wu, and C. K. Liu. Object motion guided human motion synthesis. *ACM Trans. Graph.*, 42(6), 2023.
- [25] Y. Li, J. L. Fu, and N. S. Pollard. Data-driven grasp synthesis using shape matching and task-based pruning. *IEEE Transactions on Visualization and Computer Graphics*, 13(4):732–747, 2007.
- [26] H. Liu, C. Li, Q. Wu, and Y. J. Lee. Visual instruction tuning. *Advances in neural information processing systems*, 36, 2024.
- [27] T. Liu, Z. Liu, Z. Jiao, Y. Zhu, and S.-C. Zhu. Synthesizing diverse and physically stable grasps with arbitrary hand structures using differentiable force closure estimator. *IEEE Robotics and Automation Letters*, 7(1):470–477, 2021.
- [28] X. Liu and L. Yi. Geneoh diffusion: Towards generalizable hand-object interaction denoising via denoising diffusion. *arXiv preprint arXiv:2402.14810*, 2024.
- [29] N. Mahmood, N. Ghorbani, N. F. Troje, G. Pons-Moll, and M. J. Black. Amass: Archive of motion capture as surface shapes. In *International Conference on Computer Vision (ICCV)*, pages 5442–5451, 2019.
- [30] A. Mir, X. Puig, A. Kanazawa, and G. Pons-Moll. Generating continual human motion in diverse 3d scenes. *arXiv preprint arXiv:2304.02061*, 2023.
- [31] R. OpenAI. Gpt-4 technical report. arxiv 2303.08774. *View in Article*, 2(5), 2023.
- [32] X. Peng, Y. Xie, Z. Wu, V. Jampani, D. Sun, and H. Jiang. Hoi-diff: Text-driven synthesis of 3d human-object interactions using diffusion models. *arXiv preprint arXiv:2312.06553*, 2023.
- [33] N. S. Pollard and V. B. Zordan. Physically based grasping control from example. In *Proceedings of the 2005 ACM SIGGRAPH/Eurographics symposium on Computer animation*, pages 311–318, 2005.
- [34] S. Prokudin, C. Lassner, and J. Romero. Efficient learning on point clouds with basis point sets. In *International Conference on Computer Vision (ICCV)*, pages 4332–4341, 2019.
- [35] A. Radford, J. W. Kim, C. Hallacy, A. Ramesh, G. Goh, S. Agarwal, G. Sastry, A. Askell, P. Mishkin, J. Clark, et al. Learning transferable visual models from natural language supervision. In *International conference on machine learning*, pages 8748–8763. PMLR, 2021.
- [36] A. Rodriguez, M. T. Mason, and S. Ferry. From caging to grasping. *The International Journal of Robotics Research*, 31(7):886–900, 2012.
- [37] O. Taheri, V. Choutas, M. J. Black, and D. Tzionas. Goal: Generating 4d whole-body motion for hand-object grasping. In *Conference on Computer Vision and Pattern Recognition (CVPR)*, pages 13263–13273, 2022.

- [38] O. Taheri, N. Ghorbani, M. J. Black, and D. Tzionas. GRAB: A dataset of whole-body human grasping of objects. In *European Conference on Computer Vision (ECCV)*, 2020.
- [39] O. Taheri, Y. Zhou, D. Tzionas, Y. Zhou, D. Ceylan, S. Pirk, and M. J. Black. Grip: Generating interaction poses using latent consistency and spatial cues. *arXiv preprint arXiv:2308.11617*, 2023.
- [40] P. Tendulkar, D. Surís, and C. Vondrick. Flex: Full-body grasping without full-body grasps. In *Proceedings of the IEEE/CVF Conference on Computer Vision and Pattern Recognition*, pages 21179–21189, 2023.
- [41] N. Wake, A. Kanehira, K. Sasabuchi, J. Takamatsu, and K. Ikeuchi. Gpt-4v (ision) for robotics: Multimodal task planning from human demonstration. *arXiv preprint arXiv:2311.12015*, 2023.
- [42] J. Wang, Y. Rong, J. Liu, S. Yan, D. Lin, and B. Dai. Towards diverse and natural scene-aware 3d human motion synthesis. In *Conference on Computer Vision and Pattern Recognition (CVPR)*, pages 20460–20469, 2022.
- [43] J. Wang, H. Xu, J. Xu, S. Liu, and X. Wang. Synthesizing long-term 3d human motion and interaction in 3d scenes. In *Conference on Computer Vision and Pattern Recognition (CVPR)*, pages 9401–9411, 2021.
- [44] R. Wang, J. Zhang, J. Chen, Y. Xu, P. Li, T. Liu, and H. Wang. Dexgraspnet: A large-scale robotic dexterous grasp dataset for general objects based on simulation. In *2023 IEEE International Conference on Robotics and Automation (ICRA)*, pages 11359–11366. IEEE, 2023.
- [45] Z. Wang, Y. Chen, B. Jia, P. Li, J. Zhang, J. Zhang, T. Liu, Y. Zhu, W. Liang, and S. Huang. Move as you say, interact as you can: Language-guided human motion generation with scene affordance. *arXiv preprint arXiv:2403.18036*, 2024.
- [46] Z. Wang, Y. Chen, T. Liu, Y. Zhu, W. Liang, and S. Huang. Humanise: Language-conditioned human motion generation in 3d scenes. In *Advances in Neural Information Processing Systems (NeurIPS)*, 2022.
- [47] Q. Wu, Y. Shi, X. Huang, J. Yu, L. Xu, and J. Wang. Thor: Text to human-object interaction diffusion via relation intervention. *arXiv preprint arXiv:2403.11208*, 2024.
- [48] Y. Wu, J. Wang, Y. Zhang, S. Zhang, O. Hilliges, F. Yu, and S. Tang. Saga: Stochastic whole-body grasping with contact. In *European Conference on Computer Vision (ECCV)*, pages 257–274, 2022.
- [49] Z. Xiao, T. Wang, J. Wang, J. Cao, W. Zhang, B. Dai, D. Lin, and J. Pang. Unified human-scene interaction via prompted chain-of-contacts. In *The Twelfth International Conference on Learning Representations*, 2024.
- [50] S. Xu, Z. Li, Y.-X. Wang, and L.-Y. Gui. Interdiff: Generating 3d human-object interactions with physics-informed diffusion. In *Proceedings of the IEEE/CVF International Conference on Computer Vision*, pages 14928–14940, 2023.
- [51] S. Xu, Z. Wang, Y.-X. Wang, and L.-Y. Gui. Interdreamer: Zero-shot text to 3d dynamic human-object interaction. *arXiv preprint arXiv:2403.19652*, 2024.
- [52] Y. Ye and C. K. Liu. Synthesis of detailed hand manipulations using contact sampling. *ACM Transactions on Graphics (ToG)*, 31(4):1–10, 2012.
- [53] H. Yi, J. Thies, M. J. Black, X. B. Peng, and D. Rempé. Generating human interaction motions in scenes with text control. *arXiv preprint arXiv:2404.10685*, 2024.
- [54] Y. Zeng, M. Wu, L. Yang, J. Zhang, H. Ding, H. Cheng, and H. Dong. Distilling functional rearrangement priors from large models. *arXiv preprint arXiv:2312.01474*, 2023.
- [55] H. Zhang, Y. Ye, T. Shiratori, and T. Komura. Manipnet: neural manipulation synthesis with a hand-object spatial representation. *ACM Transactions on Graphics (ToG)*, 40(4):1–14, 2021.
- [56] K. Zhao, Y. Zhang, S. Wang, T. Beeler, and S. Tang. Synthesizing diverse human motions in 3d indoor scenes. *arXiv preprint arXiv:2305.12411*, 2023.
- [57] Y. Zhou, C. Barnes, J. Lu, J. Yang, and H. Li. On the continuity of rotation representations in neural networks. In *Computer Vision and Pattern Recognition (CVPR)*, 2019.